FOCUS ISSUE OF SELECTED PAPERS FROM IMLB 2016 WITH INVITED PAPERS CELEBRATING 25 YEARS OF LITHIUM ION BATTERIES

Palladium-Filled Carbon Nanotubes Cathode for Improved Electrolyte Stability and Cyclability Performance of Li-O_2 Batteries

Neha Chawla,[=,*] Amir Chamaani,[=,*] Meer Safa,[*] and Bilal El-Zahab[z]

Department of Mechanical and Materials Engineering, Florida International University, Miami, Florida 33174, USA

Li–oxygen (Li-O_2) cathodes using palladium-coated and palladium-filled carbon nanotubes (CNTs) were investigated for their battery performance. The full discharge of batteries in the 2–4.5 V range showed 6-fold increase in the first discharge cycle of the Pd-filled over the pristine CNTs and 35% increase over their Pd-coated counterparts. The Pd-filled also exhibited improved cyclability with 58 full cycles of 500 mAh $\cdot$ g^{-1} at current density of 250 mA $\cdot$ g^{-1} versus 35 and 43 cycles for pristine and Pd-coated CNTs, respectively. In this work, the effect of encapsulating the Pd catalysts inside the CNTs proved to increase the stability of the electrolyte during both discharging and charging. Voltammetry, Raman spectroscopy, FTIR, XRD, UV/Vis spectroscopy and visual inspection of the discharge products using scanning electron microscopy confirmed the improved stability of the electrolyte due to this encapsulation and suggest that this approach could lead increasing the Li-O_2 battery capacity and cyclability performance.

Manuscript submitted September 30, 2016; revised manuscript received December 14, 2016. Published December 31, 2016. This was Paper 390 presented at the Chicago, Illinois, Meeting of the IMLB, June 19–24, 2016. *This paper is part of the Focus Issue of Selected Papers from IMLB 2016 with Invited Papers Celebrating 25 Years of Lithium Ion Batteries.*

High energy density batteries have garnered much attention in recent years due to their demand in electric vehicles. Lithium oxygen (Li-O_2) batteries have nearly 10 times the theoretical specific energy of common lithium-ion batteries and in that respect have been regarded as the batteries of the future.[1–3] A typical Li-O_2 battery consists of Li anode, porous cathode open to, oxygen and Li^+ ion conducting electrolyte separating the electrodes. Li-O_2 battery stores energy via a simple electrochemical reaction ($2Li + O_2 \leftrightarrow Li_2O_2$) in which Li_2O_2 is deposited on the surface of cathode via the forward reaction (oxygen reduction reaction, ORR) during discharge and backward reaction (oxygen evolution reaction, OER) takes place during charging to decompose Li_2O_2 on the surface of cathode.[2] Since the main discharge product (Li_2O_2) and other discharge/charge byproducts in Li-O_2 batteries are electrically insulating and not soluble in electrolytes, the structure and electronic conductivity of cathode materials have been critical factors in determining the limiting capacity of Li-O_2 batteries.[4,5] Carbonaceous materials such as carbon nanoparticles,[6,7] carbon nanofibers,[8,9] carbon nanotubes,[7,8,10] graphene platelets,[11,12] and other forms of carbons[13,14] have been commonly used as cathode materials in Li-O_2 batteries. Among carbon-based materials, carbon nanotubes (CNTs) have been widely used in Li-O_2 cathodes due to their high specific surface area, good chemical stability, high electrical conductivity, and large accessibility of active sites.[15,16] Zhang et al. reported one of the early uses of CNT (single-walled) as cathode materials in Li-O_2 batteries in which discharge specific capacities as high as 2540 mAh $\cdot$ g^{-1} were obtained at 0.1 mA $\cdot$ cm^{-2} discharge current density.[8] Although many research studies have been done to improve the performance metrics of Li-O_2 batteries, they are still in their early stages and many technical challenges have to be addressed before their practical applications.[17,18] The most common problems impeding the development of Li-O_2 batteries have been low rate capability, poor recyclability and low round-trip efficiency.[19,3] All of these issues are originally stemmed from sluggish kinetics and irreversible characteristic of the OER and ORR reactions which causes high overpotentials in discharging/charging process. Hence, increasing the efficiency of OER/ORR reactions and minimizing the overpotentials during the discharging/charging process have been regarded as a meaningful approach to overcome the aforementioned problems in Li-O_2 batteries. Various additives have been explored to remedy this problem including the use of redox mediators.[20] Redox mediators minimize charge polarization by acting as charge carriers between the cathode and Li_2O_2 surface.[21] Alternatively, the use of different noble metals and metal oxide catalysts has also been integrated in the cathodes of Li-O_2 batteries.[22–25] The catalyst may influence the performance of Li-O_2 batteries by destabilizing the oxidizing species which decreases the charging overpotential.[26,27] They may also increase the surface active sites and facilitate charge transport from oxidized reactants to the electrode which could also lead to formation of nanocrystalline Li_2O_2.[14] However, it has been recently shown that the catalyst on the oxygen cathode in Li-O_2 batteries is easily deactivated due to continuous accumulation of discharge and charge products upon cycling.[28,29] It also has been reported that coarsening and agglomeration of catalyst upon charging/discharging reduces the efficiency of catalyst in Li-O_2 batteries.[23,30] Besides the catalyst deactivation/agglomeration upon cycling, Gittleson et al. have also shown the impact of catalyst-electrolyte compatibility on Li-O_2 battery performance.[31,32] According to the report, platinum (Pt) and palladium (Pd) catalysts promote Li_2O_2 oxidation at low potentials but also cause electrolyte decomposition resulting in the formation of Li_2CO_3 and thus deactivating the catalysts. Advanced approaches such as dispersing catalysts in polymeric membrane over the oxygen electrode, chemically binding the catalysts on the surface of CNTs by atomic layer deposition, and encapsulation of catalysts inside carbon cathodes have been developed to overcome the deactivation and agglomeration of catalysts in Li-O_2 batteries.[33–37]

In this study, we report the effect of filling CNT with Pd nanoparticle catalysts to assist the ORR/OER reactions in Li-O_2 batteries while minimally destabilizing the electrolyte. To assess the effectiveness of this approach, various electrochemical, spectroscopic, and microscopic techniques have been used.

Experimental

Materials.—Palladium (II) chloride ($PdCl_2$, 59% Pd) was purchased from ACROS organics. Bis (trifluoromethane) sulfonamide (LiTFSI, purity > 99.95%), tetraethylene glycol dimethyl ether

[=]These authors contributed equally to this work.
[*]Electrochemical Society Student Member.
[z]E-mail: belzahab@fiu.edu

(TEGDME, purity > 99.00%), N-Methylpyrrolidine (NMP, purity > 97.00%), multi-walled carbon nanotubes (MWCNT, D = 5–20 nm, L = 5 μm, purity > 95.00% carbon basis), Titanium (IV) oxysulfate (TiOSO4) (≥29% Ti (as TiO_2) basis) and Lithium Peroxide (Li_2O_2) were purchased from Sigma-Aldrich. Carbon cloth gas diffusion layer (CCGDL, thickness ~300 μm) was purchased from Fuel Cell Earth. Lithium foil chips (purity > 99.90%) and Celgard polypropylene separator (thickness ~25 μm) were purchased from MTI Corp. Polyvinylidene fluoride (PVDF) was purchased from Alfa Aesar.

Electrode preparation.—Pd-filled MWCNTs were prepared following the procedure detailed elsewhere.[38] Briefly, capped MWCNTs were first decapped by nitric acid solution treatment and then 1 mM aqueous solution of $PdCl_2$ was used to swell 100 mg of decapped MWCNTs until a slurry was formed. Pd-coated CNTs were also prepared following the same procedure on untreated capped MWCNTs. Both slurries of Pd-coated and Pd-filled MWCNTs were dried overnight at room temperature and calcinated in air at 350°C for 2 hours. Corresponding particles were then hydrogenated in an oven under hydrogen gas to yield ~5 wt% Pd nanoparticles.[38] Cathodes were prepared by coating a slurry of MWCNT (Pristine, Pd-filled and Pd-coated)/PVDF (90/10 Wt% in NMP) on 0.5" diameter carbon cloth gas diffusion layer (CCGDL) followed by drying at 120°C for 12 hours. The cathodes were then stored in an Ar-filled glove box to be used later. The typical loading of MWCNT was 0.5 ± 0.01 mg. All reported capacities in this manuscript are reported per total mass of active cathode (CNTs and catalyst).

Electrolyte and battery test assembly.—The electrolyte was prepared by adding 1 $mol.kg^{-1}$ of LiTFSI salt into TEGDME solvent. Li-O_2 batteries were assembled using a Swagelok type cell with stainless steel rod on the anode side and a stainless steel tube on the cathode side. Lithium metal disc was used as anode, covered by electrolyte-soaked Celgard 2400 separator, MWCNT-CCGDL and a stainless steel mesh as a current collector. Li-O_2 batteries were rested inside Ar-filled glove box overnight before electrochemical tests. All electrolyte preparation and cell assembly were performed inside Ar-filled glove box (<1 ppm O_2 and < 0.1 ppm H_2O).

Characterization.—The Li-O_2 batteries were removed from argon glove box and placed in the gastight desiccator filled with ultra-high purity oxygen gas (Airgas, purity > 99.994%). The batteries were rested under oxygen for 5 hours before testing. Solartron 1470 battery tester was used for galvanostatic discharge/charge tests within a voltage range of 2.0–4.5 V at a current density of 250 $mA \cdot g^{-1}$. Voltammetry measurements were performed by an electrochemical workstation (Gamry reference 600) at the rate of 1 $mV \cdot s^{-1}$ in the range of 2.0–4.5 V to investigate the catalytic behavior of oxygen electrodes. All charge/discharge and electrochemical tests were measured in a temperature controlled environment at 25°C. After charge/discharge cycling, the oxygen cathodes were recovered from the batteries in the Ar-filled glove box, rinsed with acetonitrile and dried under vacuum. Cathodes were investigated by Raman spectroscopy (BaySpec's Nomadic, excitation wavelength of 532 nm), Fourier transform infrared (FTIR) spectroscopy (JASCO FT-IR 4100), and Scanning electron microscopy (SEM) (JEOL 6330F). Bruker GADDS/D8 X-ray powder diffraction (XRD) with MacSci rotating Molybdenum anode (λ = 0.71073) operated at 50 kV generator and 20 mA current was also used to collect the diffraction patterns. A parallel X-ray beam in size of 100 μm diameter was directed on to the samples and diffraction intensities were recorded on large 2D image plate during exposure time. Li_2O_2 was quantified in the cathodes after discharge using a colorimetric method previously reported by Schwenke et al.[39] Briefly, discharged cathodes were first immersed in water then aliquots were taken and added to 2% aqueous solution of $TiOSO_4$. Instantaneously a color change occurred and the absorbance spectra of the solutions were collected using a UV-Vis spectrophotometer (Gamry UV/Vis Spectro-115E). The peak intensity at 408 nm was calibrated against solutions with known concentrations of Li_2O_2, in the range of 0.1 to 10 mg/ml and linear calibration curve was obtained. Transmission Electron Microscopy (Phillips CM-200 200 kV) was also used to inspect the carbon nanotubes.

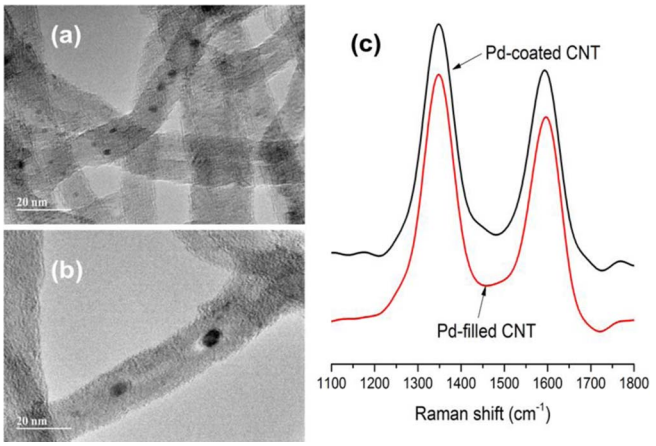

Figure 1. Transmission electron micrographs of Pd-coated CNTs (a) and Pd-filled CNTs (b). (c) Raman spectra of Pd-filled and Pd-coated CNTs.

Results and Discussion

The cathodes used in this study were composed of MWCNTs (pristine, Pd-coated and Pd-filled) coated on the woven carbon cloth gas diffusion layer (CCGDL). Homogenous three-dimensional networks of carbon nanotubes over CCGDL yields high surface area with an open structure which improves the electronic contact during charging and discharging processes.[40] Figures 1a and 1b show TEM images of Pd-coated and Pd-filled CNTs, respectively. In Pd-filled cathodes, Pd nanocatalysts are formed in the inner tubular region of decapped CNTs.[41] Figure 1c shows the Raman spectra of the Pd-coated and Pd-filled CNTs. D and G bands of Pd-filled and Pd-coated CNTs were identical in location and intensity ratios [I(G)/I(D) ~1.2] indicating that the decapped CNTs does not have high density of defects on their surface.

The first discharge and charge behaviors of Pd-coated, Pd-filled and pristine CNTs batteries using 1 M LiTFSI in TEGDME electrolyte in the voltage window of 2.0–4.5 vs Li/Li^+ at the constant

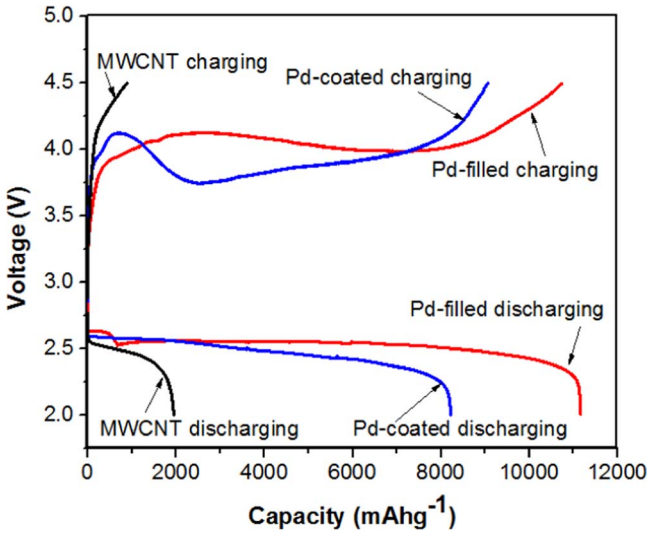

Figure 2. First discharge/charge capacity of pristine CNTs, Pd-coated CNTs and Pd-filled CNTs at a constant current density of 250 $mAh \cdot g^{-1}$ between 2.0–4.5 V.

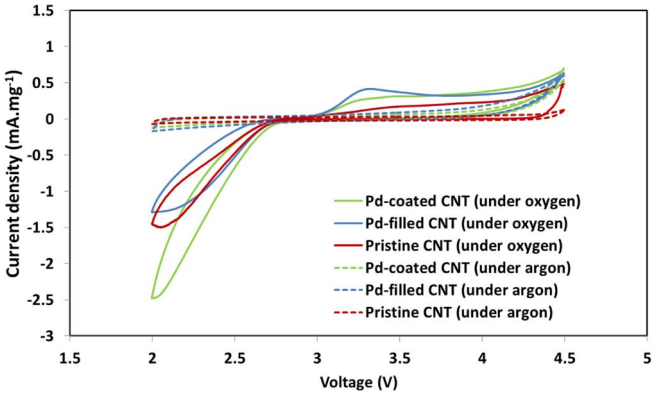

Figure 3. Cyclic voltammetry of pristine, Pd-filled, and Pd-coated CNTs in range of 2–4.5 V vs Li/Li$^+$. All scans rates 1 mV.s^{-1} under O_2 or Ar atmospheres.

current density of 250 mA · g^{-1} are shown in Figure 2. The pristine CNTs show a first discharge capacity of 1980 mAh · g^{-1} compared to 8197 mAh · g^{-1} and 11,152 mAh · g^{-1} for the Pd-coated and Pd-filled CNTs, respectively. The ∼6-fold discharge capacity improvement of Pd-coated CNTs over pristine CNTs resulted from improved ORR and increased surface sites for lithium discharge product deposition due to the presence of Pd nanocatalysts. Cyclic voltammetry (CV) measurements (Figure 3) confirm higher ORR and OER currents for Pd containing CNTs over pristine CNTs. This also confirms retained catalytic activity of Pd when encapsulated inside the CNTs, consistent with previously observations.[36,42,35] In addition, the presence of Pd nanocatalysts in both Pd-filled and Pd-coated CNTs shifts the onset of ORR peak of pristine CNTs from 2.8 V to 2.9 V, showing enhanced cathodic activity.[43] The Pd-filled CNTs also demonstrated 36% increase in first discharge capacity over Pd-coated. In the Figure 3, an oxidation peak at ∼3.3 V is attributed to the OER and was shown to be more pronounced for the Pd-filled compared to Pd-coated. It is considered that the presence of Pd inside the CNTs strengthens the π electron density on the CNT surface yielding homogeneously distributed nucleation sites for Pd-filled CNTs compared to heterogeneously distributed nucleation sites for Pd-coated CNTs.[35] This delocalization of Li_2O_2 seeding sites contributes to intimate contact between Li_2O_2 and CNTs and helps promote the formation of high surface discharge products. At voltage exceeding 3.7 V vs Li/Li$^+$ Pd-coated CNTs shows the highest rate of oxidation of electrolyte and electrolyte decomposition products.[31,32,44–46] The subtle OER activity in CV was previously reported by Gittleson et al. using TEGDME electrolyte in the presence of the noble metal catalysts.[31] Raman spectroscopic characterization on discharged cathodes revealed Li_2O_2 formation at ∼790 cm^{-1} Raman shift[47] for all discharged cathodes (Figure 4a). However, the Pd-coated CNTs cathode showed a pronounced Raman shift peak at 1080 cm^{-1}, which corresponds to the electrolyte decomposition product Li_2CO_3.[47,48] This peak was absent from pristine CNT cathodes. This behavior confirms the observation from CV, indicating reduced electrolyte stability due to the presence of Pd on Pd-coated CNTs and enhanced electrolyte stability for Pd-filled compared to Pd-coated CNTs. Following charging, Raman spectroscopic analyses on the cathodes revealed efficient removal of the Li_2O_2 peaks from all cathodes, and a decrease in peak intensity of Li_2CO_3 peak for the Pd containing CNTs. The decrease in Li_2CO_3 was previously reported to be enabled in catalyst-containing cathodes.[49] Li_2O_2 content in the cathode was quantified using a colorimetric approach previously reported by Schwenke et al.[39] The amounts of Li_2O_2 in the cathode were determined to be 11.6, 21.4, and 35.4 μmols for pristine, Pd-coated, and Pd-filled CNT cathodes, respectively. These amounts corresponded to capacity yields of approximately 88%, 23%, and 37% of the experimental capacities recorded by the pristine, Pd-coated, and Pd-filled CNT cathodes, respectively. In order to determine the molar ratio of Li_2O_2 in the discharged cathodes, the cathodes were analyzed using FTIR following the method reported by Qiao and Ye.[50] Using peak intensities ratio at 600 cm^{-1} (Li_2O_2) and 862 cm^{-1} (Li_2CO_3), Pd-coated and Pd-filled cathodes had 19.3% and 33.2% Li_2O_2 by mole, respectively. By only considering the Li_2O_2 and Li_2CO_3 discharge species, this observation is in agreement with the UV-Vis quantification and further confirms the stabilizing effect of the encapsulation of Pd inside the CNTs compared to coating the CNTs. The CV and Raman data also back up these claims, indicating that the electrolyte undergoes more decomposition in cells with Pd-coated CNTs cathodes. The presence of Li_2O_2 and Li_2CO_3 was additionally confirmed by XRD (Figure 4b).

The formation of discharge products was visually confirmed using scanning electron microscopy on discharged cathodes shown in Figure 5. The discharge products (Li_2O_2) of pristine CNTs (Figure 5a) were conformal around the cathode in rod-like structures with low porosity. The growth of layers in this morphology often yields to passivation and blockage of oxygen to the cathode and eventually limits the discharge capacity and cycle life of the battery.[51] The Pd-coated CNTs cathode (Figure 5b) show some platelet-shaped Li_2O_2 buried by thick conformal layer, suspected to be Li_2CO_3 as shown in Raman and FTIR measurements. In contrast, the Pd-filled CNTs

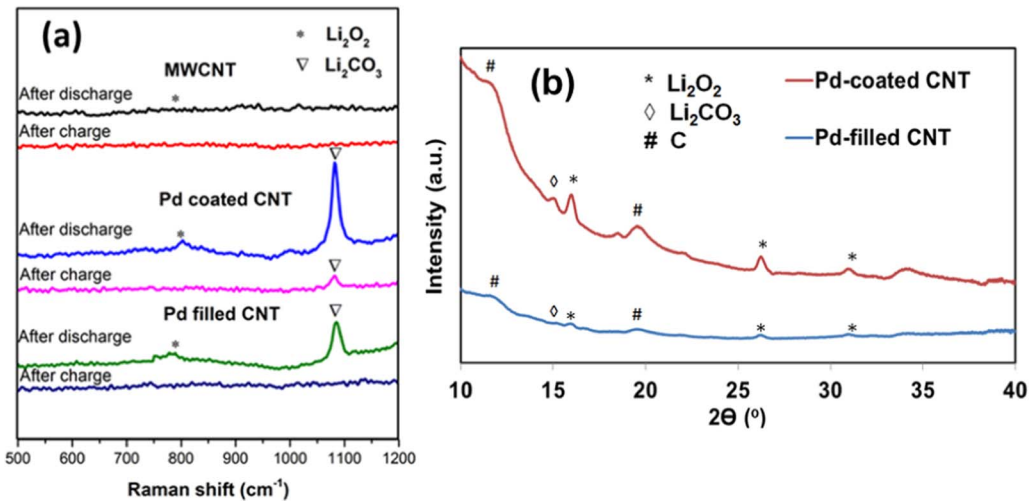

Figure 4. (a) Raman spectra after discharging and charging the batteries for pristine, Pd-coated, and Pd-filled CNTs. (b) X-ray diffraction patterns confirming the presence of Li_2O_2 and Li_2CO_3 in Pd-coated and Pd-filled discharged cathodes.

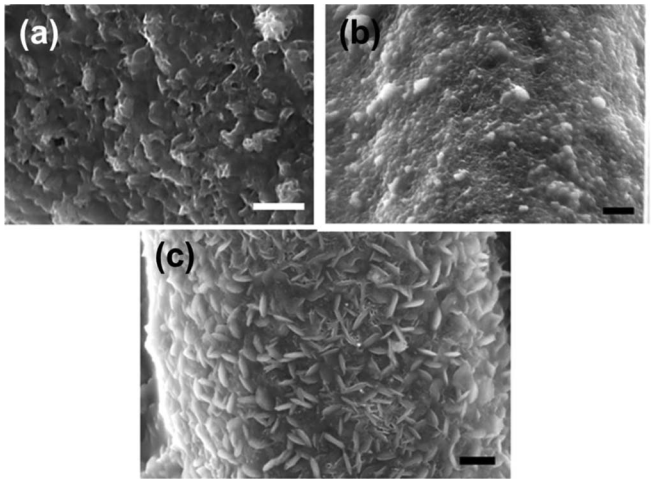

Figure 5. Scanning electron micrographs of cathodes after discharge for pristine CNTs (a), Pd-coated CNTs (b), and Pd-filled CNTs (c). The scale bars are 1 μm.

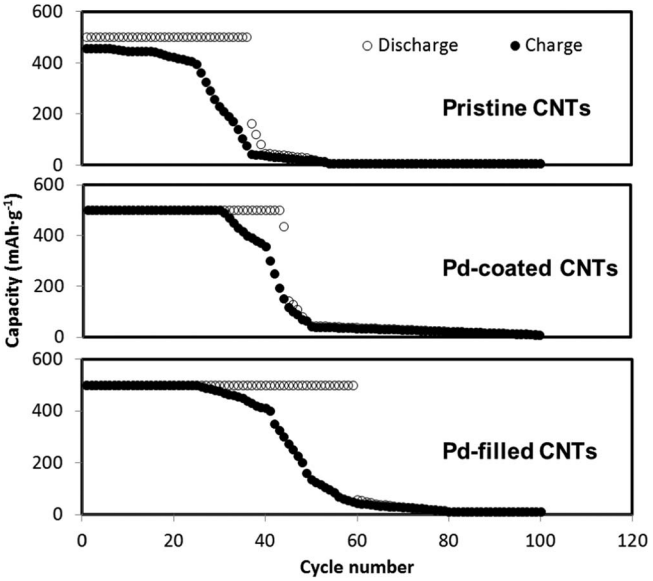

Figure 7. Cyclability of the Li-O_2 batteries for fixed cycle capacities of 500 mAh · g^{-1} at a current density of 250 mA · g^{-1} and with voltage cutoffs of 2.0–4.5 V for pristine CNTs, Pd-coated CNTs, and Pd-filled CNTs. The markers ○ denote discharge capacity and ● denote charge capacity.

show nano-thin platelets of Li_2O_2 covering the cathode (Figure 5c). These platelets of Li_2O_2 yield high surface porosity which in turn do not block the access to the CNTs and enhance the performance.

In order to identify the synergy of electrolyte and Pd nanocatalysts, the oxidation stability limit of the electrolyte was determined using a chronopotentiometric stability test and linear sweep voltammetry under oxygen atmosphere. Batteries using Pd-coated, Pd-filled and pristine CNTs were assembled and charged without prior discharging at constant current density of 250 mA · s^{-1} up to cutoff voltage of 4.5 V. Figure 6 shows higher capacity for Pd-coated compared to Pd-filled and pristine. Since no discharge products existed, the capacities obtained are attributed to electrolyte and cathode undesirable reactions. Again, this supports the claim that Pd-filled promote better stability than Pd-coated CNT cathodes. This observation was also confirmed using linear sweep voltammetry following a discharge showing increased OER peak intensity at 3.3–3.4 V and improved electrolyte stability above 3.7 V vs Li/Li^+ for Pd-filled vs Pd-coated CNTs (Figure 6b). These results again support previous observations that encapsulating the Pd nanocatalyst helped improve the electrolyte stability during the operation of the Li-O_2 battery.

The cycling stability of Li-O_2 batteries based on Pd-filled, Pd-coated, and pristine CNTs have been investigated and shown in Figure 7. Galvanostatic discharge/charge cycling of Li-O_2 batteries at a current density of 250 mA · g^{-1} at a limited capacity of 500 mAh · g^{-1} in a voltage window of 2.0–4.5 V vs Li/Li^+ were conducted. Li-O_2 cells using Pd-filled CNTs show the highest discharge cycling performance of 58 cycles compared to 43 cycles for Pd-coated, and 35 for pristine CNTs. The cycling stability improvement in the case of Pd-coated and Pd-filled CNTs is a result of previously confirmed OER/ORR improvement due to the Pd nanocatalysts. The cycling stability improvement of Pd-filled CNTs over the Pd-coated CNTs was ultimately credited to the decrease in undesirable discharge/charge products formation, e.g. Li_2CO_3, afforded by the encapsulation approach.

Conclusions

The inclusion of Pd catalyst in CNTs for use as cathode materials in Li-O_2 batteries has been demonstrated. Using two modes of CNT loading, inside (Pd-filled CNTs) and outside (Pd-coated CNTs), showed that both approaches yielded significant improvement in full discharge capacities of the batteries while the Pd-filled cycled for 35% more cycles of 500 mAh · g^{-1} at current density of 250 mA · g^{-1}. The encapsulation of nanocatalyst inside the CNTs improved the stability

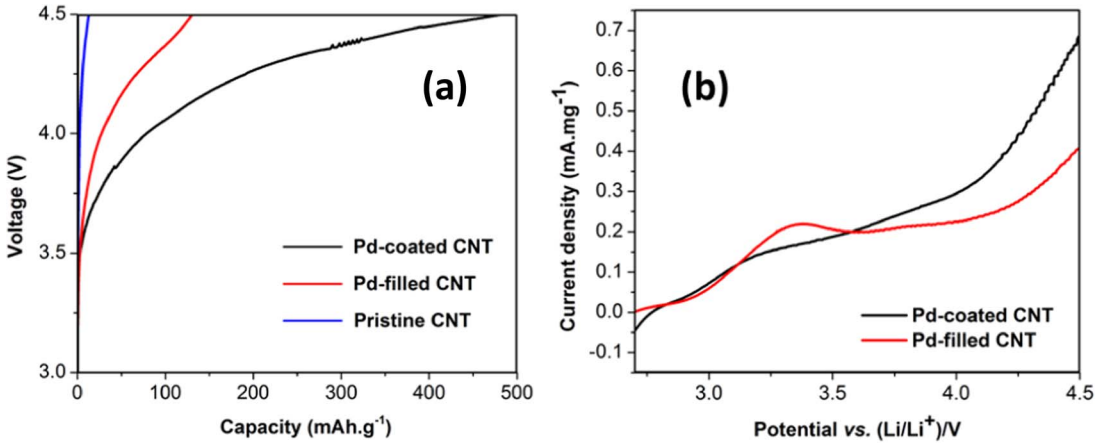

Figure 6. (a) Chronopotentiometric test at 250 mA · g^{-1} from OCV to 4.5 V for pristine, Pd-coated, and Pd-filled CNTs. (b) Linear sweep voltammetry of pre-discharged Pd-coated and Pd-filled CNTs under oxygen between OCV and 4.5 V vs Li/Li^+ at scan rate of 1 mV.s^{-1}.

of the electrolyte by decreasing the formation of Li_2CO_3 compared to nanocatalyst-coated CNTs. These observations were confirmed by voltammetry, Raman and UV/Vis spectroscopy, FTIR, chronopotentiometry, electron microscopy, and charge/discharge cycling.

Acknowledgments

The authors acknowledge the staff of the Advance Materials Engineering Research Institute (AMERI) at FIU for the assistance in electron microscopy. The authors also thank Dr. Vadym Drozd and the staff of the Center for the Study of Matter at Extreme Conditions (CeSMEC) for their assistance in the Raman spectroscopy and XRD analyzes and Richa Agrawal and Prof. Peggy Wang for their assistance in FTIR measurements. A. C. also acknowledges the financial support of a Florida International University Dissertation Year Fellowship.

References

1. K. M. Abraham and Z. Jiang, *J. Electrochem. Soc.*, **143**, 1 (1996).
2. G. Girishkumar, B. McCloskey, A. C. Luntz, S. Swanson, and W. Wilcke, *J. Phys. Chem. Lett.*, **1**, 2193 (2010).
3. P. G. Bruce, S. A. Freunberger, L. J. Hardwick, and J.-M. Tarascon, *Nat. Mater.*, **11**, 172 (2011).
4. C. Xia et al., *ACS Appl. Mater. Interfaces*, **6**, 12083 (2014).
5. V. Viswanathan et al., *J. Chem. Phys.*, **135**, 0 (2011).
6. Y. Zhang et al., *J. Power Sources*, **240**, 390 (2013).
7. R. E. Fuentes, H. R. Colón-Mercado, and E. B. Fox, *J. Power Sources*, **255**, 219 (2014).
8. G. Q. Zhang et al., *J. Electrochem. Soc.*, **157**, A953 (2010).
9. R. R. Mitchell, B. M. Gallant, C. V. Thompson, and Y. Shao-Horn, *Energy Environ. Sci.*, **4**, 2952 (2011).
10. Y. Li et al., *Electrochem. commun.*, **13**, 668 (2011).
11. Y. Li et al., *Electrochem. commun.*, **18**, 12 (2012).
12. C. Zu, L. Li, L. Qie, and A. Manthiram, *J. Power Sources*, **284**, 60 (2015).
13. T. Zhang and H. Zhou, *Nat. Commun.*, **4**, 1817 (2013).
14. J. Lu et al., *Nat. Commun.*, **4**, 2383 (2013). http://www.ncbi.nlm.nih.gov/pubmed/23986151.
15. B. Astinchap et al., *Chem. Mater.*, **24**, 3393 (2012).
16. D. M. Itkis et al., *Nano Lett.*, **13**, 4697 (2013).
17. N. Feng, P. He, and H. Zhou, *Adv. Energy Mater.*, **6**, 1 (2016).
18. D. Geng et al., *Adv. Energy Mater.*, 1 (2016).
19. J. Wang, Y. Li, and X. Sun, *Nano Energy*, **2**, 443 (2013).
20. D. Kundu, R. Black, B. Adams, and L. F. Nazar, *ACS Cent. Sci.*, **1**, 510 (2015).
21. B. J. Bergner et al., *ACS Appl. Mater. Interfaces*, **8**, 7756 (2016).
22. M. A. Rahman, X. Wang, and C. Wen, *J. Appl. Electrochem.*, **44**, 5 (2013).
23. E. Yilmaz, C. Yogi, K. Yamanaka, T. Ohta, and H. R. Byon, *Nano Lett.*, **13**, 4679 (2013).
24. B. Sun, P. Munroe, and G. Wang, *Sci. Rep.*, **3**, 1 (2013).
25. A. Débart, A. J. Paterson, J. Bao, and P. G. Bruce, *Angew. Chemie Int. Ed.*, **47**, 4521 (2008).
26. K. P. C. Yao et al., *Energy Environ. Sci.*, **8**, 2417 (2015).
27. K. P. C. Yao et al., *Phys. Chem. Chem. Phys.*, **16**, 2297 (2014).
28. Z. Jian et al., *Angew. Chem. Int. Ed. Engl.*, **53**, 442 (2014).
29. G. Gnana kumar, M. Christy, H. Jang, and K. S. Nahm, *J. Power Sources*, **288**, 451 (2015).
30. X. Yao, Q. Cheng, J. Xie, Q. Dong, and D. Wang, *ACS Appl. Mater. Interfaces*, **7**, 21948 (2015).
31. F. S. Gittleson, R. C. Sekol, G. Doubek, M. Linardi, and A. D. Taylor, *Phys. Chem. Chem. Phys.*, **16**, 3230 (2014).
32. F. S. Gittleson, W.-H. Ryu, M. Schwab, X. Tong, and A. D. Taylor, *Chem. Commun.*, **52**, 6605 (2016).
33. W. H. Ryu, F. S. Gittleson, M. Schwab, T. Goh, and A. D. Taylor, *Nano Lett.*, **15**, 434 (2015).
34. M. A. Schroeder et al., *Chem. Mater.*, **27**, 5305 (2015).
35. X. Huang et al., *Adv. Funct. Mater.*, **24**, 6516 (2014).
36. X. Guo et al., *Adv. Mater.*, **27**, 6137 (2015).
37. J. Huang et al., *Carbon N. Y.*, **100**, 329 (2016).
38. J.-P. Tessonnier, L. Pesant, G. Ehret, M. J. Ledoux, and C. Pham-Huu, *Appl. Catal. A Gen.*, **288**, 203 (2005).
39. K. U. Schwenke, M. Metzger, T. Restle, M. Piana, and H. A. Gasteiger, *J. Electrochem. Soc.*, **162**, A573 (2015).
40. H.-D. Lim et al., *Angew. Chemie Int. Ed.*, **53**, 3926 (2014).
41. S. Hevia et al., *Nanoscale Res. Lett.*, **7**, 342 (2012).
42. J. Deng et al., *Energy Environ. Sci.*, **7**, 1919 (2014).
43. Y. C. Lu, H. A. Gasteiger, and Y. Shao-Horn, *J. Am. Chem. Soc.*, **133**, 19048 (2011).
44. S. Huang, W. Fan, X. Guo, F. Meng, and X. Liu, *ACS Appl. Mater. Interfaces*, **6**, 21567 (2014).
45. R. A. Segura et al., *Nanoscale Res. Lett.*, **9**, 1 (2014).
46. W. Fan, X. Guo, D. Xiao, and L. Gu, *J. Phys. Chem. C*, **118**, 7344 (2014).
47. F. S. Gittleson et al., *ChemElectroChem*, **2**, 1446 (2015).
48. W. Xu et al., *J. Power Sources*, **215**, 240 (2012).
49. M. Hong, H. C. Choi, and H. R. Byon, *Chem. Mater.*, **27**, 2234 (2015).
50. Y. Qiao and S. Ye, *J. Phys. Chem. C*, **120**, 8033 (2016).
51. J. Hou, M. Yang, M. W. Ellis, R. B. Moore, and B. Yi, *Phys. Chem. Chem. Phys.*, **14**, 13487 (2012).